

Improved Dirichlet boundary conditions for lattice gauge-fermion theories

Tobias Rindlisbacher*

*Albert Einstein Center for Fundamental Physics & Institute for Theoretical Physics,
University of Bern, Sidlerstrasse 5, CH-3012 Bern, Switzerland*

Kari Rummukainen† and Ahmed Salami‡

*Department of Physics & Helsinki Institute of Physics,
University of Helsinki, P.O. Box 64, FI-00014 University of Helsinki, Finland*

Hybrid Monte Carlo (HMC) simulations of lattice gauge theories with fermionic matter rely on the invertibility of the lattice Dirac operator. Near-zero modes of the latter can therefore significantly slow down the update algorithm and cause instabilities. This is in particular a problem when dealing with massless fermions. Homogeneous temporal Dirichlet boundary conditions can be used to remove zero modes from massless lattice Dirac operators, but the standard implementation of these boundary conditions can cause severe finite-volume cutoff effects in regions of parameter space where the physics at the ultraviolet (UV) cutoff scale is dominated by the fermionic instead of the gauge action. In lattice quantum chromodynamics (QCD) this is usually not an issue, as the gauge action dominates the UV physics and the problem does not show up. In studies of beyond standard model (BSM) theories, on the other hand, the finite-volume artifacts can be severe. We have identified the origin of these IR cutoff effects and propose a simple improvement on the homogeneous temporal Dirichlet boundary conditions to prevent them. We demonstrate the benefits of using our improved boundary conditions at the example of $SU(2)$ lattice gauge theory with $N_f = 24$ massless Wilson-clover flavors. Due to the large number of fermions in this theory, the boundary-related finite volume artifacts are particularly strong, and the effect from switching from the normal to our improved homogeneous Dirichlet boundary conditions is therefore distinct.

I. INTRODUCTION

Temporal Dirichlet boundary conditions (TDBs) are widely used in lattice studies of quantum chromodynamics (QCD) and related quantum field theories (QFTs). The corresponding Euclidean path integrals are known as "Schrödinger functionals" (SF) and have certain appealing features: appropriately chosen boundary conditions induce a background field in the bulk, which can be used to define a non-perturbative running coupling [1], the so-called SF coupling. Furthermore, the use of TDBs removes zero modes from massless lattice Dirac operator [2], which is important for hybrid Monte Carlo (HMC) simulations of gauge-fermion theories, as the HMC update method relies on the invertibility of the lattice Dirac operator, and becomes unstable if the latter has near-zero eigenvalues.

TDBs for pure $SU(N)$ lattice gauge theories were introduced in ref. [1] and extended to incorporate Wilson-Dirac [3] and $\mathcal{O}(a)$ improved Wilson-clover [4] fermions in ref. [2]. Here a is the lattice spacing. Straightforward implementation of TDBs gives rise to $\mathcal{O}(a)$ cutoff effects, which can be compensated by introducing boundary counterterms for the fermion and gauge part of the action. The coefficients of the counterterms have been evaluated in perturbation theory for $SU(2)$ and $SU(3)$ pure gauge theory [1, 5] and with fundamental representation fermions [6–8]. These calculations were extended to higher fermion representations in refs. [9, 10] and to higher $SU(N)$ groups in

ref. [11]. The boundary improvement for Symanzik improved gauge action and clover fermions was discussed in [12–14].

Since the introduction of gradient flow (GF) techniques [15] in lattice studies, the GF coupling proposed in [16] has to a large extent replaced the background field SF coupling as the preferred definition of a non-perturbative running coupling on the lattice. SF boundary conditions are, however, still widely used in lattice studies of gauge theories with massless fermions in order to prevent instabilities due to near-zero Dirac-eigenvalues.

The improvement of the GF in combination with SF boundary conditions is discussed in [17]. Unfortunately these improvement techniques rely on perturbation theory and are applicable only if the bare lattice gauge coupling is sufficiently small. In QCD-like theories the gauge coupling becomes small as the distance scale is reduced, and hence the bare lattice gauge coupling can be kept small. However, large bare gauge couplings are met in theories where the coupling runs slowly, for example in studies of theories featuring an infrared fixed point.

In the non-perturbative regime, the naive use of unimproved SF boundary conditions can cause severe lattice artifacts, in particular if the physics at the UV cutoff scale is not dominated by the gauge action but significantly affected by the presence of fermion fields. While these artifacts, as we will illustrate, seem to be caused by the UV-details of the lattice implementation of the TDBs, they manifest themselves most prominently in the form of severe infrared-cutoff effects in the gradient flow (see Fig. 6), and can therefore have implications for studies of the non-perturbative running of the coupling in gauge-fermion theories. In this paper we present a straightforward improvement of standard TDBs, and show that these remove the

* trindlis@itp.unibe.ch

† kari.rummukainen@helsinki.fi

‡ ahmed.salami@helsinki.fi

harmful lattice artifacts.

The remainder of this paper is organized as follows: Sec. II introduces the lattice actions and observables that will be used in the forthcoming sections. In Sec. III we discuss the standard implementation of homogeneous TDBs for $SU(N)$ lattice gauge theories with Wilson-Dirac fermions. We explain why this implementation can give rise to severe infrared (IR) cutoff effects and how these manifest in gradient flow studies. In Sec. IV we introduce the improved boundary conditions and show that the discussed cutoff effects are removed. Concluding remarks and a brief outlook to future studies are given in Sec. V.

II. LATTICE FORMALISM

In this section we provide some details on the utilized lattice actions and observables. All quantities are dimensionless, meaning that the lattice representation of physical quantities with a non-trivial mass dimension are implicitly multiplied with an appropriate power of the lattice spacing, a , to render the product dimensionless. For a mass or energy, we have for example: $m = a\tilde{m}$ and $E = a\tilde{E}$; for the field strength: $F_{\mu\nu} = a^2\tilde{F}_{\mu\nu}$, and for a position vector: $x_\mu = \tilde{x}_\mu/a$, and so on, where the quantities with a tilde are the non-lattice ones, which have their natural mass dimension.

A. Lattice actions

In this section we describe the lattice gauge and fermion actions used to perform the HMC updates. For the gauge part we use Wilson's $SU(N)$ lattice gauge action [3],

$$S_G = \frac{\beta_L}{N} \sum_x \sum_{\mu < \nu} \text{Re Tr}(\mathbb{1} - U_{\mu\nu}(x)), \quad (1)$$

with $\beta_L = 2N/g_0^2$ being the bare inverse gauge coupling and $U_{\mu\nu}(x) \in SU(N)$ are the so-called plaquette variables, given by

$$U_{\mu\nu}(x) = U_\mu(x)U_\nu(x + \hat{\mu})U_\mu^\dagger(x + \hat{\nu})U_\nu^\dagger(x). \quad (2)$$

The link variables, $U_\mu(x) \in SU(N)$, can be written as

$$U_\mu(x) = \exp(iA_\mu(x)), \quad (3)$$

with $A_\mu(x) \in \mathfrak{su}(N)$ being the μ -component of the lattice gauge field, which is assumed to be constant along the link that connects the site x to its nearest neighboring site in μ -direction, $x + \hat{\mu}$.

For the fermion part we use the Wilson-clover action [4],

$$S_F = \sum_{f=1}^{N_f} \sum_{x,y} \bar{\psi}_x^{(f)} \left(D_{x,y}^{(f)}[U] + C_{x,y}^{(f)}[U] \right) \psi_y^{(f)}, \quad (4)$$

where for each flavor f , $D^{(f)}[U]$ is the Wilson-Dirac operator for the given set of gauge link variables, $U =$

$\{U_\mu(x)\}_{\forall x,\mu}$, and $C^{(f)}[U]$ is the corresponding clover operator. The two operator can be written as,

$$D_{x,y}^{(f)}[U] = \delta_{x,y} \mathbb{1} - \kappa_f \sum_{\mu=1}^4 (\delta_{x+\hat{\mu},y} (\mathbb{1} - \gamma_\mu) U_\mu(x) + \delta_{x-\hat{\mu},y} (\mathbb{1} + \gamma_\mu) U_\mu^\dagger(x - \hat{\mu})), \quad (5)$$

and

$$C_{x,y}^{(f)}[U] = c_{SW} \kappa_f \delta_{x,y} \frac{1}{2} \sum_{\mu < \nu} [\gamma_\mu, \gamma_\nu] P_{\mu\nu}(x). \quad (6)$$

In Eqs. (5) and (6) $\kappa_f = 1/(2m_{f,0} + 8)$ is the hopping parameter for the flavor f , encoding the flavor's bare fermion mass, $m_{f,0}$, the parameter $c_{SW} = 1 + \mathcal{O}(g_0^2)$ is the Sheikholeslami-Wohlert coefficient, and $P_{\mu\nu}(x)$ the clover term [4], defined as,

$$P_{\mu\nu}(x) = \frac{1}{4} (U_\mu(x)U_\nu(x + \hat{\mu})U_\mu^\dagger(x + \hat{\nu})U_\nu^\dagger(x) - U_\nu^\dagger(x - \hat{\nu})U_\mu^\dagger(x - \hat{\mu} - \hat{\nu})U_\nu(x - \hat{\mu} - \hat{\nu})U_\mu(x - \hat{\mu}) + U_\nu(x)U_\mu^\dagger(x - \hat{\mu} + \hat{\nu})U_\nu^\dagger(x - \hat{\mu})U_\mu(x - \hat{\mu}) - U_\mu(x)U_\nu^\dagger(x + \hat{\mu} - \hat{\nu})U_\mu^\dagger(x - \hat{\nu})U_\nu(x - \hat{\nu})), \quad (7)$$

and which is a lattice approximation of the field strength tensor $F_{\mu\nu}(x) = P_{\mu\nu}(x) + \mathcal{O}(a^2)$.

B. Gradient flow and observables

The gradient flow [15] of the gauge field is performed with the Lüscher-Weisz action [18] and we monitor three different observables of the flow-evolved gauge field as functions of the flow time t resp. the corresponding flow scale $\lambda = \sqrt{8t}$. The first of these observables is the rescaled plaquette action density,

$$\langle s_U(x, t) \rangle = t^2 \langle \text{Re Tr}(\mathbb{1} - U_{\mu\nu}(x, t)) \rangle / N, \quad (8)$$

where $U_{\mu\nu}(x, t)$ is the plaquette variable from Eq. (2) for the flow-evolved gauge link variables at flow time t . The second observable is the topological charge or instanton density,

$$\langle q_{\text{topo}}(x, t) \rangle = \frac{1}{32\pi^2} \epsilon_{\mu\nu\rho\sigma} \langle \text{Tr}(P_{\mu\nu}(x, t)P_{\rho\sigma}(x, t)) \rangle, \quad (9)$$

with $P_{\rho\sigma}(x, t)$ being the clover term from Eq. (6) for the flow-evolved gauge link variables at flow time t . The third observable is the gradient flow gauge coupling [15], defined as

$$g_{\text{GF}}^2(\lambda) = \frac{2\pi^2 \lambda^4 \langle E(\lambda) \rangle}{3(N^2 - 1)(1 + \delta_{L/a}(\lambda/L))}, \quad (10)$$

with $\langle E(\lambda) \rangle$ being the average clover gauge action density at flow time t and $\delta_{L/a}(\lambda/L)$ a finite-volume correction factor [16, 19]. To minimize boundary effects from the

TDBs, the action density $\langle E(\lambda) \rangle$ is evaluated on the hyperplane where $x_4 = N_t/2$. We will also show results for the topological susceptibility,

$$\chi_{\text{topo}} = \langle Q_{\text{topo}}^2 \rangle - \langle Q_{\text{topo}} \rangle^2, \quad (11)$$

with the topological charge given in terms of Eq. (9) as,

$$Q_{\text{topo}} = \sum_x q_{\text{topo}}(x, t_{L/2}), \quad (12)$$

where $t_{L/2}$ is the flow time t for which the flow scale $\lambda = \sqrt{8t}$ equals $L/2$.

III. HOMOGENEOUS TEMPORAL DIRICHLET BOUNDARY CONDITIONS

A typical implementation of homogeneous TDBs in $SU(N)$ lattice gauge theory with Wilson-Dirac fermions, described by the Dirac operator in Eq. (5), is illustrated in Fig. 1 for the case of trivial boundary fields: the spatial gauge links within the boundary layers at $x_4 = 0$ and $x_4 = N_t$, where N_t is the temporal size of the lattice, are set to the identity, and the fermion fields are required to vanish on the boundary¹. This is sufficient to remove near-zero modes from the Wilson-Dirac operator [2] and to thereby stabilize the HMC update algorithm.

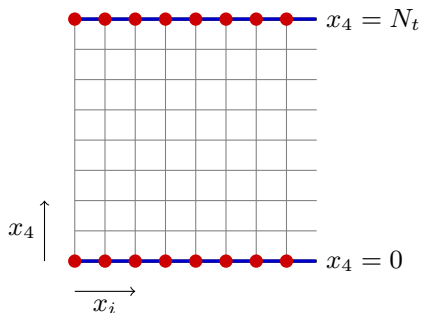


Figure 1. Illustration of (ordinary) homogeneous temporal Dirichlet boundary conditions (TDBs) with trivial boundary fields: spatial gauge links within the boundary layers at $x_4 = 0, N_t$ (blue links) are set to the identity, while the fermion fields are required to vanish on the boundary (red dots).

For QCD or QCD-like lattice theories, where the physics at the UV-cutoff scale is for most of the simulation parameter space governed by the gauge action and controlled by the inverse bare gauge coupling, $\beta_L = 2N/g_0^2$, these boundary conditions are usually well behaved [1, 5,

¹ The implementation of TDBs for Wilson-Dirac fermions, as presented in [2], requires in principle only to fix half of the fermionic degrees of freedom on the boundary. However, as also the gauge field is held fixed along the boundary, the remaining fermionic boundary degrees of freedom have no opportunity to interact with the bulk system and can therefore, without loss of generality, be set to zero.

6, 8] and can even be further improved [12] to match bulk actions with reduced UV-cutoff effects [4, 18, 20, 21].

The boundary conditions can, however, cause problems in theories in which the fermionic action has a dominant effect on the UV physics, or in regions of parameter space of QCD-like theories, where the gauge action becomes subdominant. The latter can be the case, if the inverse bare gauge coupling, β_L , is too small, so that the Wilson gauge action from Eq. (1) does no longer sufficiently constrain the values of the traces of the plaquette variables in Eq. (2). Then, the behavior of the gauge field at the plaquette-level (i.e. UV-cutoff scale) is dictated by the interaction of the gauge field with the fermions.

A. Why do the boundary conditions fail?

It is well known that the Wilson and Staggered fermion actions induce a term which is proportional to the plaquette gauge action [22–24], and therefore introduce a shift in the effective inverse gauge coupling:

$$\beta_{L,\text{eff}} = \beta_L + \Delta\beta_L, \quad (13)$$

where $\Delta\beta_L \propto N_f$. If the bare gauge coupling is very strong, the shift $\Delta\beta_L$ can dominate $\beta_{L,\text{eff}}$.

The reason why the TDBs from Fig. 1 may cause problems is illustrated in Fig. 2. The requirement for the fermion fields to vanish on the $x_4 = 0$ and $x_4 = N_t$ boundaries implies that the fermion “hopping terms” along temporal links connecting to either of the boundaries (dashed, orange lines) vanish. This means that there are no fermion loops around temporal plaquettes which touch the boundary (blue squares) and hence the increase in effective β_L due to fermions is strongly suppressed.

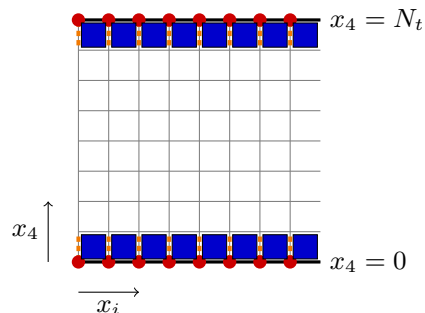


Figure 2. Illustration of the problem caused by the trivial temporal Dirichlet boundary conditions (TDBs) from Fig. 1: as the fermion fields are required to vanish on the boundaries at $x_4 = 0, N_t$, fermion hopping is prevented along the temporal links that connect to the boundaries (orange, dashed links). Consequently, the effect of the fermion fields on gauge links that are part of temporal boundary plaquettes (blue squares) is significantly smaller on gauge links deeper in the bulk.

Thus, the boundary plaquettes are effectively at much stronger coupling than the plaquettes in the bulk. As will be demonstrated below, this has an effect in the measurement of the gradient flow coupling. If the bare lattice coupling is weak, the shift can be compensated in perturbation

theory [6–11]. At strong coupling, however, the perturbative improvement is not sufficient.

B. Example: severe boundary effects in SU(2) with $N_f = 24$ massless fermions

To provide a concrete example, we consider here a SU(2) lattice gauge theory with Wilson plaquette gauge action from Eq. (1) and $N_f = 24$ massless (in terms of PCAC mass [7]), fundamental Wilson-clover fermions with action as in Eq. (4) and with Sheikholeslami-Wohlert coefficient $c_{\text{SW}} = 1$ [25]. The fermions couple to hypercubically truncated stout-smearred (HEX-smearred) [26] gauge links. The theory is not asymptotically free, but it is still of interest to observe the behaviour of the theory at strong coupling in the light of asymptotic safety [27–29].

In previous lattice studies of the model [29–31] the requirement of strong effective coupling (small $\beta_{L,\text{eff}}$) forced one to use even negative values for the bare inverse gauge coupling β_L . Indeed, in ref. [29] it was estimated that $\beta_{L,\text{eff}} \approx 0.7$ with the bare $\beta_L = -0.3$.

The boundary effect can be clearly observed in Fig. 3, which shows measurements of the average temporal (panel (a)) and average spatial (panel (b)) plaquettes per time slice, obtained from a HMC simulation of the SU(2), $N_f = 24$ theory at $\beta_L = -0.3$. The temporal plaquettes at the boundary have a negative value, as expected for negative β_L in absence of the fermion-induced shift $\Delta\beta_L$ from Eq. (13).

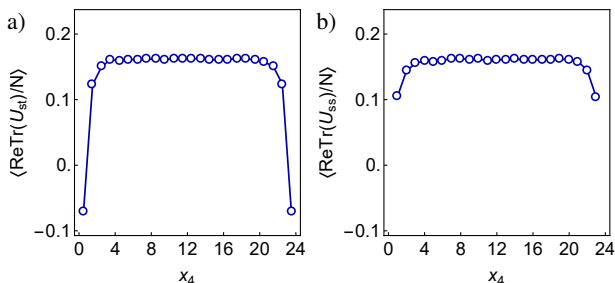


Figure 3. Average temporal (a) and spatial (b) plaquette per time slice (labeled by x_4) for a SU(2) lattice gauge theory with $N_f = 24$ massless (w.r.t. PCAC mass) Wilson-clover flavors, measured at $\beta_L = -0.3$ on a $L^4 = 24^4$ lattice with the boundary conditions from Fig. 1. The spatial plaquette values at $x_4 = 0, 24$ are not shown as the boundary conditions require them to be unity. The temporal plaquettes at the boundary have a negative value, as expected for negative bare β_L if the fermion-induced $\Delta\beta_L$ (cf. Eq. (13)) is absent.

While Fig. 3 seems to indicate that the boundary effects vanish quickly with increasing distance from the boundary, their presence can in fact severely affect measurements of bulk quantities. The reason for this is, that the strongly fluctuating gauge field at the boundary can easily induce topology changes via instanton/anti-instanton creation/annihilation. Although these instantons mostly remain localized near the boundary during the simulation,

the Dirichlet boundary conditions do not allow the instantons to disappear through the boundary during the gradient flow. Consequently, the excess energy stored within these instantons has to dissipate in the bulk under the action of the gradient flow, either in the form of remnant heat instanton/anti-instanton pairs that annihilate under the action of the flow, or in the form of stable instantons, which the flow pushes away from the flat TDBs.

This is visualized in Fig. 4, which shows how the rescaled plaquette action density from Eq. (8) (panels (a)-(d)) and the topological charge distribution from Eq. (9) (panels (e)-(h)) in a typical configuration at $\beta_L = -0.3$ evolve under the gradient flow.

Panels (a) and (d) show, respectively, how the average rescaled plaquette action per x_4 - and x_1 -slice changes as function of flow scale $\lambda = \sqrt{8}t$, with t being the gradient flow time, while panel (b) shows how the quantity is distributed as function of both, x_1 and x_4 at the value of λ that is indicated by the grey lines in panels (a) and (d) (i.e. at $\lambda = N_t/2 = 12$). The plots in (c) represent, respectively, the cross-sections along the grey lines in (a) and (d).

The panels (e)-(h) represent analogously the data for the corresponding topological charge per x_4 - and x_1 - slice as function of λ . These show that with increasing flow scale the instantons indeed appear near the boundaries and then move slowly away from them. No instantons show up directly from within the bulk. The latter suggests that in Fig. 5 the non-zero topological susceptibility at small β_L is primarily a boundary artifact. Since SU(2) gauge theory with $N_f = 24$ fundamental, massless fermion flavors is an IR-free theory [30, 31], one would indeed expect the topological susceptibility to vanish.

The presence of the artificial instantons slows down the decay of the action density under the effect of the gradient flow, so that $t^2 \text{Re Tr}(\mathbb{1} - U_{\mu\nu})$ in panels (a)-(d) of Fig. 4 grows rapidly as function of flow time t in the region where the instantons are located.

Although the upper plot of panel (c) in Fig. 4 indicates that the peaks in the action-distribution are still around $x_4 = 3$ and $x_4 = 21$ for $\lambda = 12$, the excess action due to instantons has indeed already reached the central time slice and is the reason for severe IR-cutoff effects in the gradient flow running coupling shown in Fig. 6: as the gradient flow scale, λ , approaches the value $N_t/2$, the gradient flow coupling, g_{GF}^2 , from Eq. (10) starts to increase rapidly. The theory is infrared free, and the physical coupling is expected to decrease with the distance scale (λ). The rapid increase of the coupling is an unphysical finite volume effect, which can be seen from the fact that the length scale where the coupling starts to increase grows as the volume increases. This effect cannot be compensated by the finite volume correction discussed in Eq. (10).

IV. IMPROVED HOMOGENEOUS DIRICHLET BOUNDARY CONDITIONS

In the previous section we have seen that the homogeneous TDBs from Fig. 1 can cause severe problems in lattice

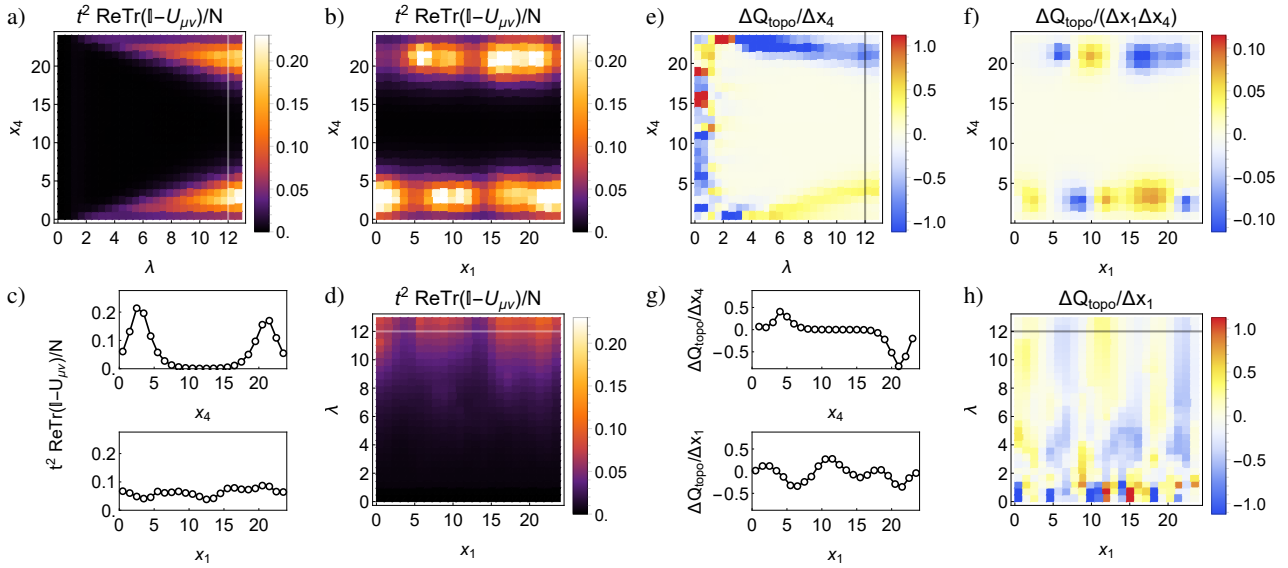


Figure 4. Illustration of how the rescaled plaquette action density (panels (a)-(d)) and topological charge distribution (panels (e)-(h)) in a typical configuration, obtained at $\beta_L = -0.3$ with the homogeneous temporal Dirichlet boundaries (TDBs) from Fig. 1, evolve under the gradient flow. The Dirichlet boundaries are located at $x_4 = 0, N_t$, where $N_t = 24$, and $\lambda = \sqrt{8t}$ is the gradient flow scale after flow time t . Panels (a) and (d) show, respectively, how the average re-scaled plaquette action per x_4 - and x_1 -slice changes as function of λ , while panel (b) shows how the quantity is distributed as function of both, x_1 and x_4 at the value of λ that is indicated by the grey lines in panels (a) and (d). The plots in (c) represent the cross-sections along the grey lines in (a) and (d). The panels (e)-(h) represent analogously the data for the corresponding topological charge.

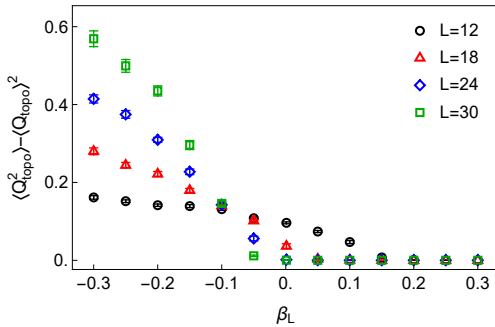


Figure 5. Topological susceptibility form Eq. (11) for SU(2) lattice gauge theory with $N_f = 24$ massless Wilson-clover fermions as function of β_L for four different system sizes $V = L^4$ with $L = 12, 18, 24, 30$ and homogeneous temporal Dirichlet boundary conditions (TDBs). The non-zero topological susceptibility at strong coupling is merely due to the artificial instanton/anti-instanton production at the boundaries.

simulations of gauge-fermion theories if the simulation parameters are such that the physics at the UV-cutoff scale is predominantly governed by the fermionic instead of the gauge action. These are caused by the fact that the boundary conditions strongly reduce the effect of the fermion action on the plaquettes touching the boundary.

A simple way to regulate the behaviour of the gauge field on the temporal boundary plaquettes is to simply freeze the involved gauge links, by setting them all to unity:

$$U_{x,i=1,2,3} = \mathbb{1} \quad \text{if} \quad x_4 \in \{0, 1, N_t - 1, N_t\}, \quad (14a)$$

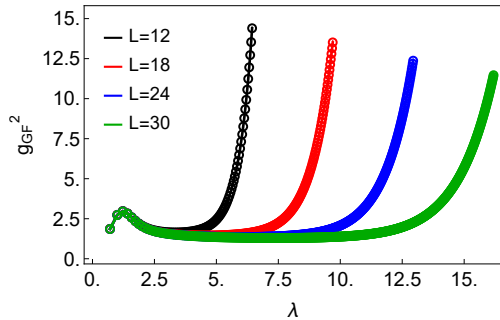


Figure 6. Gradient flow coupling, g_{GF}^2 , from Eq. (10), as function of flow scale, λ , for SU(2) lattice gauge theory with $N_f = 24$ massless Wilson-clover fermions at $\beta_L = -0.3$ for four different system sizes $V = L^4$ with $L = 12, 18, 24, 30$ and homogeneous temporal Dirichlet boundary conditions (TDBs). The rapid increase of g_{GF}^2 when λ approaches $L/2$ is a pure finite-volume artifact, caused by the naive implementation of the TDBs.

$$U_{x,4} = \mathbb{1} \quad \text{if} \quad x_4 \in \{0, N_t - 1\}. \quad (14b)$$

The fermions are still required to vanish on the boundaries:

$$\psi_x = 0 \quad \text{if} \quad x_4 \in \{0, N_t\}, \quad (14c)$$

$$\bar{\psi}_x = 0 \quad \text{if} \quad x_4 \in \{0, N_t\}. \quad (14d)$$

These boundary conditions, to which we will refer as “thick” improved homogeneous TDBs, are graphically depicted in Fig. 7. They are particularly easy to implement in a parallel HMC code, as one can simply set the force terms for the blue-marked links in Fig. 7 to zero during the gauge

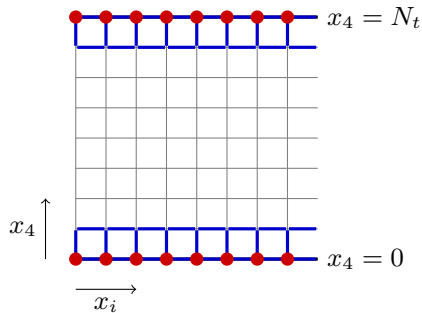


Figure 7. Improved, “thick” homogeneous temporal Dirichlet boundary conditions: all link variables that are part of temporal boundary plaquettes are set to the identity matrix (blue links). The fermion fields are required to vanish on the boundary (red dots).

update. The side effect of implementing the thick TDBs in this way is, that the active gauge field lattice volume gets reduced from $N_s^3 \times N_t$ to $V_A = N_s^3 \times (N_t - 2)$, which can be compensated by increasing the original N_t by two units.

Physically equivalent boundary condition to Eqs. (14a–14b) can also be obtained by using standard “thin” TDBs and setting β_L to infinity for plaquettes which include link variables on $x_4 = 0$ or $x_4 = N_t$. This forces the blue links in Fig. 7 to become gauge equivalent with the unit matrix. We note that the perturbative 1-loop boundary improvement due to fermions also increases the effective inverse coupling for the boundary plaquette [6–8], but at strong coupling this perturbative correction is insufficient. The goal of the perturbative improvement is also slightly different from the “thick” TDBs introduced here: the perturbative improvement aims to compensate the boundary lattice effects while keeping the original active volume from $x_4 = 0$ to N_t . In contrast, the “thick” boundary conditions Eqs. (14a–14b) exclude the boundary layers from the physical volume, reducing the active volume to the interval $1 \leq x_4 \leq N_t - 1$.

To demonstrate that the improved, “thick” TDBs, just introduced in Sec. IV, prevent the formation of the boundary artifacts discussed in Sec. III, we repeat some of the SU(2), $N_f = 24$ simulations and the related analysis.

With the “thick” temporal boundary conditions from Fig. 7, the temporal boundary plaquettes, that do not experience the fermion field, are set to unity, so that they cannot act up and give rise to any sort of non-trivial artifacts that could alter the physics in the bulk. Comparing Fig. 8 with Fig. 3, we see that the “thick” TDBs affect the average plaquette values per time slice much less than the normal TDBs did. In particular, the plaquettes near the boundary are no longer significantly shifted to smaller values, indicating that the boundary layers are no longer at stronger effective coupling than the bulk. As a consequence, the excess instanton production we observed with the ordinary TDBs (cf. in Fig. (4)), should now be absent. Fig. 9 show that the latter is indeed the case: panels (e)–(h) show that no excess instantons show up near the temporal boundaries and the rescaled action density in panels (a)–(d)

does no longer blow up near the boundary as in Fig. (4).

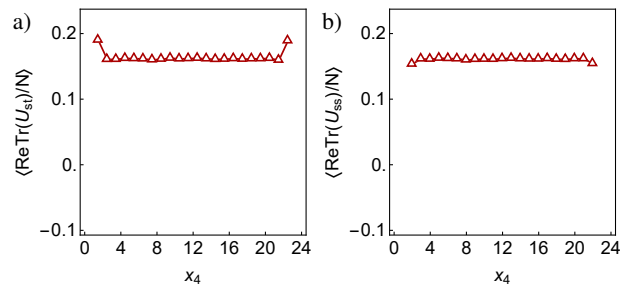


Figure 8. Average temporal (a) and spatial (b) plaquette per time slice (labeled by x_4) for a SU(2) lattice gauge theory with $N_f = 24$ massless Wilson-clover flavors, measured at $\beta_L = -0.3$ on a $L^4 = 24^4$ lattice with the improved temporal Dirichlet boundary conditions from Fig. 7. The unity plaquette values from within the boundary layers are not plotted.

In Fig. 10 we compare data for the topological susceptibility from Eq. (11) on a $L = 24$ lattice, obtained with normal and “thick” TDBs. As can be seen, with the “thick” TDBs, the topological susceptibility remains zero all the way down to $\beta_L = -0.3$, indicating that the non-zero topological susceptibility, obtained with the normal TDBs, is a consequence of the artificial instanton/anti-instanton production at the boundary.

In Fig. 11 the corresponding gradient flow running coupling, g_{GF}^2 , from Eq. (10) is shown as function of $c = \lambda/L$, for normal (blue data) and improved “thick” (red data) TDBs for $\beta_L = -0.3$ (top) and $\beta_L = 1.0$ (bottom). For the improved “thick” TDBs, the finite volume correction in Eq. (10) has been adjusted to incorporate the fact that the active volume for the gauge field is reduced by two time slices $N_t \rightarrow N_t - 2 \neq L$. As discussed in Sec. III B, in the system with normal boundary conditions, the instantons and anti-instantons produced at the boundary for $\beta_L = -0.3$ slow down the decay of the action density in the gradient flow-evolved gauge field, which spoils the definition of the running GF coupling. As soon as the flow scale, λ , of the gradient flow is sufficiently large, so that the flowed field from near the boundary reaches the central time slice at $x_4 = L/2$, where the clover action for the gradient flow coupling is measured, the latter starts to increase rapidly. With the “thick” boundary conditions, there are no boundary instantons that interfere with the gradient flow, and the definition of the gradient flow coupling remains valid when the relative flow scale $c = \lambda/L$ approaches the value $c = 0.5$. The gradient flow coupling therefore remains flat, as expected for an IR-free theory. For $\beta_L = 1.0$, the gauge action is by itself, i.e. also in the absence of fermions, able to sufficiently constrain the temporal boundary plaquettes in the system with naive DB boundary conditions, so that no excess instantons get produced. The gradient flow coupling with normal boundary conditions behaves therefore almost like the one with the “thick” boundary conditions. The remnant additional increase in the gradient flow coupling with naive DB boundary conditions can be blamed to the fact that the

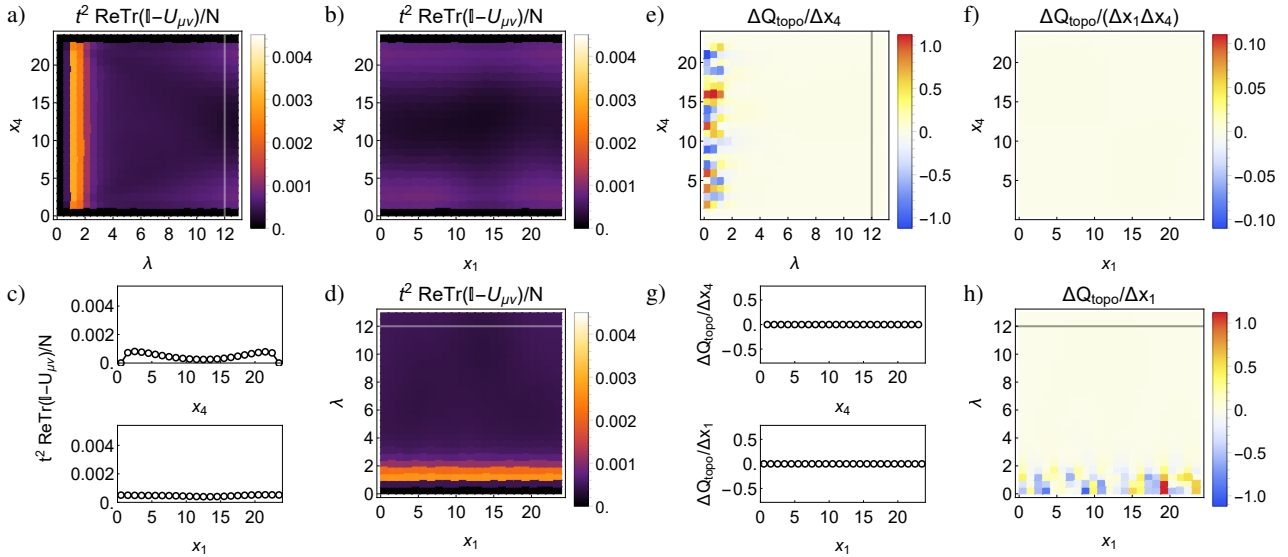


Figure 9. Illustration of how the rescaled plaquette action density (panels (a)-(d)) and topological charge distribution (panels (e)-(h)) in a typical configuration, obtained at $\beta_L = -0.3$ with thick homogeneous temporal Dirichlet boundaries, evolve under the gradient flow. The data is represented analogously as in Fig. 4.

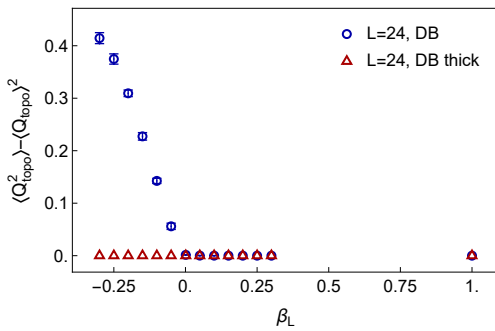


Figure 10. Topological susceptibility from Eq. (11) for SU(2) lattice gauge theory with $N_f = 24$ massless Wilson-clover fermions as function of β_L on a L^4 lattice with $L = 24$. The blue circles show the results obtained with the normal TDBs from Fig. 1, and the red triangles the corresponding results for the improved, “thick” boundary conditions (DB thick) from Fig. 7. The non-zero topological susceptibility at strong coupling for DB is merely due to the artificial instanton/anti-instanton production at the boundaries.

normal boundary conditions nevertheless tend to increase the action in the near-boundary region, while the “thick” boundary conditions tend to decrease it (compare Fig. 3 and Fig. 8).

V. CONCLUSIONS AND OUTLOOK

We have introduced modified homogeneous temporal Dirichlet boundary conditions (TDBs) for lattice studies of gauge-fermion theories at strong bare lattice gauge coupling. The boundary conditions are designed to reduce lattice artifacts caused by the TDBs, in particular for observables measured using gradient flow. We demonstrated

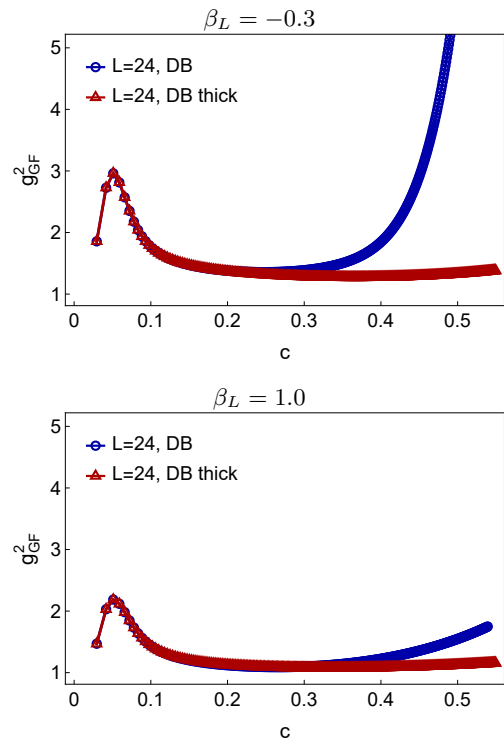


Figure 11. Gradient flow (GF) running coupling from Eq. (10) for SU(2) lattice gauge theory with $N_f = 24$ massless Wilson-clover fermions at $\beta_L = -0.3$ (top) and $\beta_L = 1.0$ (bottom) on a L^4 lattice with $L = 24$ as function of $c = \lambda/L$, where $\lambda = \sqrt{8}t$ is the flow scale at flow time t . The blue data corresponds to the GF running coupling for a system with normal temporal Dirichlet boundary conditions (cf. Fig. 1), while the red data shows the GF running coupling for a corresponding system with improved, “thick” boundary conditions (cf. Fig. 7).

that the new boundary conditions dramatically reduce the finite volume (IR-cutoff) artifacts in lattice simulations of $SU(2)$ gauge theory with $N_f = 24$ massless Wilson-clover fermions. Similar improvements are expected in other theories where the bare lattice gauge coupling is large.

Large values of the bare lattice gauge coupling have to be faced e.g. in studies of asymptotically free theories which have an infrared conformal fixed point (or are close to having one). In order to have strong effective coupling at the scale of the lattice size, it is then necessary to use large bare lattice gauge coupling, due to the very slow running of the coupling with increasing length scale. Large bare coupling values can lead to harmful discretization artifacts in the lattice gauge field. There have been recent proposals to reduce these artifacts by modifying the lattice gauge action [32–34] and to reach stronger effective cou-

pling values at weak bare coupling by introducing heavy auxiliary scalar fields [33]. The interplay of these proposals and the improved Dirichlet boundary conditions will be the subject of a future study.

VI. ACKNOWLEDGEMENT

The support of the Academy of Finland grants 345070 and 320123 is acknowledged. T. R. is supported by the Swiss National Science Foundation (SNSF) through the grant no. TMPFP2_210064. The authors wish to acknowledge CSC - IT Center for Science, Finland, for computational resources.

-
- [1] M. Luscher, R. Narayanan, P. Weisz and U. Wolff, “The Schrödinger functional: A Renormalizable probe for nonAbelian gauge theories,” Nucl. Phys. B **384** (1992), 168-228 doi:10.1016/0550-3213(92)90466-O [arXiv:hep-lat/9207009 [hep-lat]].
 - [2] S. Sint, “On the Schrodinger functional in QCD,” Nucl. Phys. B **421** (1994), 135-158 doi:10.1016/0550-3213(94)90228-3 [arXiv:hep-lat/9312079 [hep-lat]].
 - [3] K. G. Wilson, “Confinement of Quarks,” Phys. Rev. D **10** (1974), 2445-2459 doi:10.1103/PhysRevD.10.2445
 - [4] B. Sheikholeslami and R. Wohlert, “Improved Continuum Limit Lattice Action for QCD with Wilson Fermions,” Nucl. Phys. B **259** (1985), 572 doi:10.1016/0550-3213(85)90002-1
 - [5] M. Luscher, R. Sommer, P. Weisz and U. Wolff, “A Precise determination of the running coupling in the $SU(3)$ Yang-Mills theory,” Nucl. Phys. B **413** (1994), 481-502 doi:10.1016/0550-3213(94)90629-7 [arXiv:hep-lat/9309005 [hep-lat]].
 - [6] S. Sint and R. Sommer, “The Running coupling from the QCD Schrodinger functional: A One loop analysis,” Nucl. Phys. B **465** (1996), 71-98 doi:10.1016/0550-3213(96)00020-X [arXiv:hep-lat/9508012 [hep-lat]].
 - [7] M. Luscher and P. Weisz, “ $O(a)$ improvement of the axial current in lattice QCD to one loop order of perturbation theory,” Nucl. Phys. B **479** (1996), 429-458 doi:10.1016/0550-3213(96)00448-8 [arXiv:hep-lat/9606016 [hep-lat]].
 - [8] M. Luscher, S. Sint, R. Sommer and P. Weisz, “Chiral symmetry and $O(a)$ improvement in lattice QCD,” Nucl. Phys. B **478** (1996), 365-400 doi:10.1016/0550-3213(96)00378-1 [arXiv:hep-lat/9605038 [hep-lat]].
 - [9] T. Karavirta, A. Mykkanen, J. Rantaharju, K. Rummukainen and K. Tuominen, “Nonperturbative improvement of $SU(2)$ lattice gauge theory with adjoint or fundamental flavors,” JHEP **06** (2011), 061 doi:10.1007/JHEP06(2011)061 [arXiv:1101.0154 [hep-lat]].
 - [10] T. Karavirta, K. Tuominen and K. Rummukainen, “Perturbative Improvement of the Schrodinger Functional for Lattice Strong Dynamics,” Phys. Rev. D **85** (2012), 054506 doi:10.1103/PhysRevD.85.054506 [arXiv:1201.1883 [hep-lat]].
 - [11] A. Hietanen, T. Karavirta and P. Vilaseca, “Schrödinger functional boundary conditions and improvement for $N > 3$,” JHEP **11** (2014), 074 doi:10.1007/JHEP11(2014)074 [arXiv:1408.7047 [hep-lat]].
 - [12] T. R. Klassen, “The Schrodinger functional for improved gluon and quark actions,” Nucl. Phys. B **509** (1998), 391-428 doi:10.1016/S0550-3213(97)00598-1 [arXiv:hep-lat/9705025 [hep-lat]].
 - [13] S. Aoki, R. Frezzotti and P. Weisz, “Computation of the improvement coefficient $c(SW)$ to one loop with improved gluon actions,” Nucl. Phys. B **540** (1999), 501-519 doi:10.1016/S0550-3213(98)00742-1 [arXiv:hep-lat/9808007 [hep-lat]].
 - [14] S. Takeda, S. Aoki and K. Ide, “A Perturbative determination of $O(a)$ boundary improvement coefficients for the Schrodinger functional coupling at one loop with improved gauge actions,” Phys. Rev. D **68** (2003), 014505 doi:10.1103/PhysRevD.68.014505 [arXiv:hep-lat/0304013 [hep-lat]].
 - [15] M. Lüscher, “Properties and uses of the Wilson flow in lattice QCD,” JHEP **08** (2010), 071 [erratum: JHEP **03** (2014), 092] doi:10.1007/JHEP08(2010)071 [arXiv:1006.4518 [hep-lat]].
 - [16] P. Fritzsche and A. Ramos, “The gradient flow coupling in the Schrödinger functional,” JHEP **10** (2013), 008 doi:10.1007/JHEP10(2013)008 [arXiv:1301.4388 [hep-lat]].
 - [17] M. Dalla Brida *et al.* [ALPHA], “Slow running of the Gradient Flow coupling from 200 MeV to 4 GeV in $N_f = 3$ QCD,” Phys. Rev. D **95** (2017) no.1, 014507 doi:10.1103/PhysRevD.95.014507 [arXiv:1607.06423 [hep-lat]].
 - [18] M. Luscher and P. Weisz, “On-shell improved lattice gauge theories,” Commun. Math. Phys. **98** (1985) no.3, 433 [erratum: Commun. Math. Phys. **98** (1985), 433] doi:10.1007/BF01205792
 - [19] Z. Fodor, K. Holland, J. Kuti, D. Nogradi and C. H. Wong, “The Yang-Mills gradient flow in finite volume,” JHEP **11** (2012), 007 doi:10.1007/JHEP11(2012)007 [arXiv:1208.1051 [hep-lat]].
 - [20] P. Weisz, “Continuum Limit Improved Lattice Action for Pure Yang-Mills Theory. 1.,” Nucl. Phys. B **212** (1983), 1-17 doi:10.1016/0550-3213(83)90595-3

- [21] Y. Iwasaki, “Renormalization Group Analysis of Lattice Theories and Improved Lattice Action. II. Four-dimensional non-Abelian SU(N) gauge model,” [arXiv:1111.7054 [hep-lat]].
- [22] A. Hasenfratz and T. A. DeGrand, “Heavy dynamical fermions in lattice QCD,” Phys. Rev. D **49** (1994), 466-473 doi:10.1103/PhysRevD.49.466 [arXiv:hep-lat/9304001 [hep-lat]].
- [23] T. Blum, C. E. DeTar, U. M. Heller, L. Karkkainen, K. Rummukainen and D. Toussaint, “Thermal phase transition in mixed action SU(3) lattice gauge theory and Wilson fermion thermodynamics,” Nucl. Phys. B **442** (1995), 301-316 doi:10.1016/0550-3213(95)00137-9 [arXiv:hep-lat/9412038 [hep-lat]].
- [24] P. de Forcrand, S. Kim and W. Unger, “Conformality in many-flavour lattice QCD at strong coupling,” JHEP **02** (2013), 051 doi:10.1007/JHEP02(2013)051 [arXiv:1208.2148 [hep-lat]].
- [25] J. Rantaharju, T. Rantalaiho, K. Rummukainen and K. Tuominen, “Running coupling in SU(2) gauge theory with two adjoint fermions,” Phys. Rev. D **93** (2016) no.9, 094509 doi:10.1103/PhysRevD.93.094509 [arXiv:1510.03335 [hep-lat]].
- [26] S. Capitani, S. Durr and C. Hoelbling, “Rationale for UV-filtered clover fermions,” JHEP **11** (2006), 028 doi:10.1088/1126-6708/2006/11/028 [arXiv:hep-lat/0607006 [hep-lat]].
- [27] O. Antipin and F. Sannino, “Conformal Window 2.0: The large N_f safe story,” Phys. Rev. D **97** (2018) no.11, 116007 doi:10.1103/PhysRevD.97.116007 [arXiv:1709.02354 [hep-ph]].
- [28] N. A. Dondi, G. V. Dunne, M. Reichert and F. Sannino, “Analytic Coupling Structure of Large N_f (Super) QED and QCD,” Phys. Rev. D **100** (2019) no.1, 015013 doi:10.1103/PhysRevD.100.015013 [arXiv:1903.02568 [hep-th]].
- [29] V. Leino, T. Rindlisbacher, K. Rummukainen, F. Sannino and K. Tuominen, “Safety versus triviality on the lattice,” Phys. Rev. D **101** (2020) no.7, 074508 doi:10.1103/PhysRevD.101.074508 [arXiv:1908.04605 [hep-lat]].
- [30] J. Rantaharju, T. Rindlisbacher, K. Rummukainen, A. Salami and K. Tuominen, “Spectrum of SU(2) gauge theory at large number of flavors,” Phys. Rev. D **104** (2021) no.11, 114504 doi:10.1103/PhysRevD.104.114504 [arXiv:2108.10630 [hep-lat]].
- [31] T. Rindlisbacher, K. Rummukainen, A. Salami and K. Tuominen, “Nonperturbative Decoupling of Massive Fermions,” Phys. Rev. Lett. **129** (2022) no.13, 131601 doi:10.1103/PhysRevLett.129.131601 [arXiv:2110.13882 [hep-lat]].
- [32] A. Hasenfratz, “Infrared fixed point of the 12-fermion SU(3) gauge model based on 2-lattice MCRG matching,” Phys. Rev. Lett. **108** (2012), 061601 doi:10.1103/PhysRevLett.108.061601 [arXiv:1106.5293 [hep-lat]].
- [33] A. Hasenfratz, Y. Shamir and B. Svetitsky, “Taming lattice artifacts with Pauli-Villars fields,” Phys. Rev. D **104** (2021) no.7, 074509 doi:10.1103/PhysRevD.104.074509 [arXiv:2109.02790 [hep-lat]].
- [34] T. Rindlisbacher, K. Rummukainen and A. Salami, “Bulk-transition-preventing actions for SU(N) gauge theories,” Phys. Rev. D **108** (2023) no.11, 114511 doi:10.1103/PhysRevD.108.114511 [arXiv:2306.14319 [hep-lat]].